Repair of osteochondral defects in the minipig model by OPF hydrogel loaded with adipose-derived mesenchymal stem cells

Laura de Girolamo*[,1], Stefania Niada[1,2], Elena Arrigoni[2], Alessia Di Giancamillo[1,3], Cinzia Domeneghini[3], Mahrokh Dadsetan[4], Michael J Yaszemski[4], Dario Gastaldi[5], Pasquale Vena[5], Matteo Taffetani[5], Alberto Zerbi[1], Valerio Sansone[1,6], Giuseppe M Peretti[1,6] & Anna T Brini[1,2]

[1]IRCCS Istituto Ortopedico Galeazzi; Via R. Galeazzi 4, 20161 Milano, Italy

[2]Department of Biomedical, Surgical & Dental Sciences, University of Milan, Milan, Italy

[3]Department of Health, Animal Science & Food Safety, University of Milan, Milan, Italy

[4]Department of Orthopaedic Surgery, Mayo Clinic, College of Medicine, Rochester, MN, USA

[5]LaBS-Laboratory of Biological Structure Mechanics, Department of Chemistry, Materials & Chemical Engineering Giulio Natta, Politecnico di Milano, Milan, Italy

[6]Department for Biomedical Sciences for Health, University of Milan, Milan, Italy

*Author for correspondence:
Tel.: +39 02 66214059
laura.degirolamo@grupposandonato.it

The treatment of osteochondral defects represents one of the major and most problematic issues in the orthopedic practice. One of the main obstacles arises from the disparity concerning both anatomy, composition and most importantly, rate of healing of the articular cartilage (AC) and of the subchondral bone. Despite these two tissues exhibit considerably different structural composition, they constitute a single unit which acts as a whole in carrying its physiological function of absorbing mechanical stress for a suitable transmission of forces in the joints [1,2]. Furthermore, synergy between subchondral bone and AC is required for a mutual remodeling process [3]. One strategy to treat the entire osteochondral unit is the autologous or allogeneic transplantation, even though this approach presents some complications such as uneven surface, dislocation, donor site morbidity or lack of cadaveric graft [4,5]. To overcome these problems, the employment of scaffolds could represent a valid alternative. Indeed, biomaterials could be differently molded to fill properly osteochondral defect shapes and donor site morbidity is completely avoided. In the recent years, different types of cells combined with a variety of supports have been tested in many tissue engineering preclinical studies. Beside autologous chondrocytes [6,7], mesenchymal stem cells (MSCs) are an attractive alternative for the treatment of osteochondral defects. MSCs were first isolated from bone marrow [8] and, the search for MSC-like cells in specific tissues and organs has led to the discovery of a variety of progenitor cells from several adult tissues [9–11] with multi-differentiation ability toward cells of mesodermal origin, such as osteoblast- as well as chondrocytes-like cells [9]. Moreover, it has been shown in several preclinical studies, that these cells display the potential to restore and/or regenerate damaged tissues [12–14]. In particular, a great interest has been focused on cell-based therapies involving adipose-derived stem cells (ASCs). ASCs can be easily extracted with mild donor site morbidity or patient discomfort, and they showed a more potent immunomodulatory effect compared with

bone marrow-derived stem cells (BMSCs), by the secretion of higher levels of factors, such as IL-6 and TGF-β1 [15]. Moreover, the low immunogenicity of ASCs has been exploited in several studies of allogeneic transplantation, shown to be safe and without adverse reactions such as inflammation and rejection [16,17].

Concerning the regenerative treatments for osteochondral defects, biphasic scaffolds able to support the growth of cartilage and bone have been developed [18–21]. However, since the microenvironment at the injured site acts by itself as a stimulus for the regeneration, the combined use of monophasic scaffolds and progenitor cells has been demonstrated to be efficient [22,23].

In this study, critical knee osteochondral defects were treated with bioconstructs made of a hydrogel of oligo (polyethylene glycol) fumarate (OPF) combined with either autologous, allogeneic or human ASCs in Yucatan miniature swine model and evaluated at 6 months of follow-up, with the aim of proving the efficacy of this combined approach.

Materials & methods

Scaffold preparation

Oligo(polyethylene glycol) fumarate (OPF) was synthesized using polyethylene glycol (PEG) with the initial molecular weight of 10,000 as previously described [24]. Porous negatively charged hydrogels were made by dissolving 1 g OPF macromer and 0.1 g sodium methacrylate (SMA) in 2 ml deionized water containing 0.15% (w/w) Irgacure 2959 (Ciba-Specialty Chemicals, NY, USA) and 300 µl N-vinyl pyrrolidinone. In order to obtain hydrogels with 75% porosity, the resulting solution was mixed with sodium chloride (particle size, 300 µm) at a ratio of 1:3 (W/W), and polymerized using 365 nm UV light at the intensity of ~8 mW/cm^2 (Black-Ray Model 100AP, CA, USA) for 30 min. Cylindrical hydrogel scaffolds (9 mm diameter, 8 mm height) were cut using a cork borer and placed in deionized water for 48 h with four to five changes.

ASC isolation, expansion & characterization

Seven adult (12 months old) male Yucatan minipigs, with an average weight of 73.5 ± 2.2 kg (range 71–77 kg), were included in the study. Animal care and surgery were approved by the Ethical and Technical Committee of the Italian Ministry of Health (CRABCC-22–2011); all the animal experiments were performed in accordance with both policies and principles of laboratory animal care and with the European Union guidelines (86/609/EEC) approved by the Italian Ministry of Health (Law 116/92), which was effective at the time of authorization.

During the first surgical procedure, upon shaving and disinfection, adipose tissue (~8 g) was harvested from the interscapular region of all animals. General anesthesia was induced by intramuscular injection of a combination of ketamine (10 mg/kg) and midazolam (0.5 mg/kg) and maintained via inhalation of a mixture of isoflurane 4% in oxygen. The small incision was then sutured and the animals were administered once with tramadol (1 mg/kg) and meloxicam (0.4 mg/kg) to control pain.

Minipig ASCs (mpASCs) were isolated from fat tissue after 0.1% type I collagenase digestion, as previously described [25], and then purified by adhesion culturing them in DMEM supplemented with 10% fetal bovine serum, 50 U/ml penicillin, 50 µg/ml streptomycin, and 2 mM L-glutamine (Sigma–Aldrich, Milan, Italy) at 37°C in a humidified atmosphere with 5% CO_2. At 80–90% of confluence, adherent cells were detached from the culture plates by incubation with trypsin/EDTA (0.5% trypsin/0.2% EDTA; Sigma-Aldrich) for 3 min at 37°C. Cells were plated at a density of 5 × 10^3 cells/cm^2 for further expansion.

Human ASCs (huASCs) were isolated from waste adipose tissue from aesthetic liposuction of a female donor (age 61, BMI < 30 kg/m^2, no metabolic disease) after informed consent and Institutional Review Board approval (M-SPER-014.ver7 for use of surgical waste) of Galeazzi Orthopedic Institute, Milano, Italy, as previously described [26]. Human cells were obtained as porcine ASCs, with the exception of the collagenase digestion protocol (0.075%) and plating density (10^4 cells/cm^2).

Colony forming unit-fibroblast assay (CFU-F) was performed by plating in 6-well plates 1000 ASCs/well serial diluted [25,26].

For *in vitro* assessment, at passage 4, both mpASCs and huASCs were induced to differentiate toward cells of the osteogenic and chondrogenic lineages in specific culture conditions [25,27]. Osteogenic differentiation was assessed after 14 days evaluating alkaline phosphatase (ALP) activity, collagen deposition by Sirius Red staining and calcified extracellular matrix deposition by Alizarin Red S staining, as previously described [28]. Chondrogenic differentiation was determined quantifying the sulfated glycosaminoglycans (GAGs) content according to the dimethylmethylene blue modified assay [27].

Experimental design & surgical procedure

About 3 weeks after fat tissue withdrawal, 3 × 10^6 of undifferentiated either minipig or human ASCs, were seeded on each OPF cylindrical scaffold and let to adhere overnight. Cell-free scaffolds followed identical procedure. Next day, the minipigs were surgically treated under general anesthesia. With the animals in dorsal recumbence, a medial parapatellar incision and

arthrotomy were performed on the right hind leg to expose the anterior aspect of the distal femur. Using a standardized core punch, four osteochondral lesions (9 mm in diameter, 8 mm in depth each) per knee were created in the trochlea periphery (Figure 1). The 28 defects were differently treated as reported in Table 1. Untreated defects were considered the negative controls (UNT group, n = 7). Each scaffold was maintained into the lesion by press-fit.

After implantation, the joint capsule was closed and the wound was sutured in layers with bioabsorbable stitches. After surgery, the minipigs were treated at first with enrofloxacin (2 mg/kg iv.) and amoxicillin (15 mg/kg im.); then, with enrofloxacin (5 mg/kg dye for 5 days im.) and meloxicam (0.4 mg/kg dye for 3 days) to control pain. The animals were progressively allowed to free movements and carefully monitored until full recovery.

Six months later, all animals were euthanized by intravenous injection of pentothal sodium (50 mg/kg) and potassium chloride (20 mg/kg); the right hind legs were explanted and then analyzed by MRI. Then, the joints were dissected, the treated portions retrieved *en bloc* and cut into four pieces corresponding to the four osteochondral defects, to allow independent analyses of each defect. Each single defect was prepared for further analyses. The contralateral legs were also explanted and used as controls.

Macroscopic analysis

Macroscopic signs of infection, inflammation, hypertrophy of the synovial membrane and tissue adhesions were assessed. The gross chondral surface was evaluated, taking into account the neo-formed tissue and the interface implant-host tissue. Signs of incomplete filling, matrix degradation, fusion between the different osteochondral defects and other possible features were recorded.

MRI protocol

The right hindlimb of all animals and one control left limb were imaged by MRI. Examinations were performed using two 1.5 T magnetic field super conducting MR Systems (Avanto, Siemens Medical Solution, Erlangen, Germany, gradient strength 45 mT/m, slew rate 200 T/m/ms, with a dedicated eight-channel knee coil, Invivo, FL, USA).

The hindlimbs of minipigs were positioned with the knee extended and with the joint space in the middle of the coil. Lesions were studied with the following sequences:

- PD-TSE FS SPACE sequence on sagittal plane (repetition time [RT]/echo time [ET]: 1200/35; field of view [FOV]: 170 × 170 mm; matrix: 320 × 320; slice thickness: 1 mm; voxel size: 0.5 × 0.5 × 1 mm; number of slice: 60; scan time: 9 min, 2 s);
- T2-weighted TSE sequence on sagittal plane (RT/TE: 3300/83; flip angle: 150°; FOV: 180 × 180 mm; matrix: 320 × 320; slice thickness: 3 mm; voxel size: 0.6 × 0.6 × 3 mm; number of slice: 20; scan time: 4 min, 1 s);
- T1-weighted Vibe Water Excitation (WE) GE sequence on sagittal plane (RT/TE: 15.6/6.65; Flip angle: 12°; FOV: 200 × 160 mm; Matrix: 256 × 256; slice thickness: 1 mm; voxel size: 0.8 × 0.8 × 1 mm; number of slice: 72; scan time: 5 min, 45 s);
- T1-weighted sequence on sagittal plane (RT/TE: 560/10; flip angle: 143°; FOV: 160 × 160 mm; matrix: 384 × 310; slice thickness: 2.5 mm; voxel size: 0.5 × 0.4 × 2.5 mm; number of slice: 20; scan time: 5 min, 14 s).

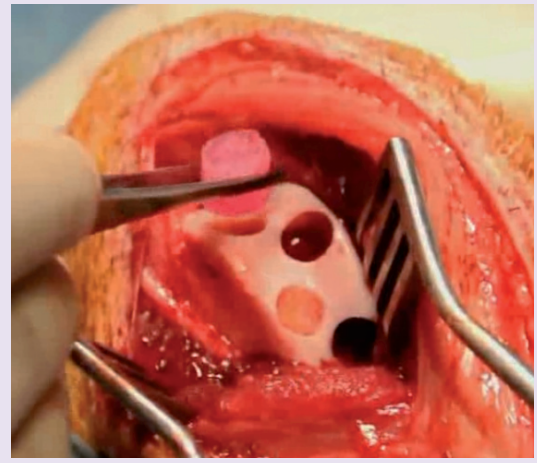

Figure 1. Surgical technique and constructs implantation. Osteochondral lesions in the trochlea periphery of the knee joint of a minipig.

Table 1. Experimental scheme: groups of treatment for the 28 critical osteochondral defects in the minipigs' right knees.

Treatment	n
Untreated (UNT)	7
Unseeded scaffold (OPF)	7
OPF + autologous ASCs (OPF-A)	7
OPF + allogeneic ASCs (OPF-Allo)	3
OPF + human ASCs (OPF-Hu)	4

ASC: Adipose-derived stem cell; OPF: Oligo(polyethylene glycol)fumarate; UNT: Untreated.

Postprocessing was performed on a dedicated workstation (Leonardo, Siemens Medical Solution, Forchein, Germany). Image evaluations were performed by two experienced senior musculoskeletal radiologists.

MRI data were analyzed by the modified 2D MOCART score [29,30] for the evaluation of *ex vivo* osteochondral samples, as reported in Table 2. The scale ranged between 0 and 100, where 0 was the worst and 100 the best scoring.

Histological & immunohistochemical analysis

The samples were dissected free of soft tissue, fixed in 10% buffered formalin for 24 h at room temperature, and then decalcified in a formic acid-sodium citrate solution as described elsewhere [13]. After decalcification, samples were rinsed for 10 min in running water, and processed for paraffin embedding through a graded ethanol series. Four-micrometer-thick sections were obtained and stained with Safranin-O following a standard protocol, for the evaluation of the structural details and GAGs deposition. Following rehydration, sections for immunohistochemical analyses were incubated in an aqueous solution of 1% H_2O_2 for 30 min at room temperature, washed three-times in PBS and then incubated overnight with either mouse anticollagen type I antibody or anticollagen type II (both Chondrex, Inc., WA, USA; 1:500). Antigen retrieval was performed by treating the sections in citrate buffer, pH 6.0, in a microwave oven (two-times for 5 min at 500 W) for anticollagen type I and with 2% hyaluronidase solution (Sigma-Aldrich) at room temperature for 30 min for anticollagen type II. Antigen–antibody complexes were detected with a peroxidase-conjugated polymer, which carries secondary antibody molecules directed against mouse immunoglobulins

Table 2. 2D MOCART scale developed by Marlovits *et al*.[†] and modified by Goebel *et al*.[‡]

Parameter	Item	Score
Defect fill	Subchondral bone exposed	0
	Incomplete <50%	5
	Incomplete >50%	10
	Complete	20
	Hypertrophy	15
Cartilage	Complete	15
	Demarcating border visible	10
	Defect visible <50%	5
	Defect visible >50%	0
Surface	Intact	10
	Damaged <50% of depth	5
	Damaged >50% of depth	0
Adhesion	Yes	5
	No	0
Structure	Homogeneous	5
	Inhomogeneous or cleft formation	0
Signal intensity	Normal	30
	Nearly normal	10
	Abnormal	0
Subchondral lamina	Intact	5
	Nonintact	0
Subchondral bone	Intact	5
	Granulation tissue, cyst, sclerosis	0
Effusion	No	5
	Yes	0

[†]Data taken from Marlovits *et al.* [30].
[‡]Data taken from Goebel *et al.* [29].

(EnVisionTM+, DakoCytomation, Milan, Italy) applied for 60 min at room temperature. Peroxydase activity was detected with diaminobenzidine (DAB, DakoCytomation) as the substrate. For all the immunohistochemical procedures, the samples were weakly counterstained with Mayer's hematoxylin, dehydrated and permanently mounted. The specificity of anti-collagen type I or type II antibody was also assessed. Photomicrographs were taken with an Olympus BX51 microscope (Olympus, Milan, Italy) equipped with a digital camera and final magnifications were calculated. The sections were also analyzed with a polarized light microscope (Leica DM LP microscope, Leica Microsystems, Wetzlar, Germany) in order to investigate the tissue organization, referring to collagen fibers of the newly formed structures.

Histological scoring

Oriented histological specimens and stained with Safranin-O were evaluated to assess the quality of tissue repair [31]. The ICRS II scoring system was chosen [32]. It contains 14 parameters: an overall assessment and 13 parameters relating to both chondrocyte and tissue features (Table 3). Each parameter was scored using a 100 mm VAS (Visual Analog Scale), where 0 was considered as poor quality and 100 as very good quality. Three experienced blind researchers independently evaluated several sections of all the specimens for each group of treatment.

Biomechanical test by nanoindentation

The experiments were performed using a NanoTest Indenter (Micro-Materials, Ltd., Wrexham, UK) equipped with a liquid cell to keep samples in a hydrated and fully saturated state. The sample preparation protocol was the following: each sample was thawed in a thermal bath at 37°C for 45 min; the samples were glued on a cylindrical aluminum stub equipped with a glass chamber and placed into the nanoindenter; the chamber was filled with physiological solution (0.90% w/v of NaCl) and maintained to achieve the thermal and swelling equilibrium before running the tests.

Nanoindentation tests were carried out following a multiload schedule in load control mode. The maximum load was applied by a series of load steps of increment 0.1 mN with a holding time of 120 s at the end of each load level. The maximum indentation force was ranging between 0.3 and 1 mN according to the sample compliance. The loading and unloading rates were 1 mN/s and the tests were carried out with two spherical tips of radii R_{25}= 25 µm and R_{400}= 400 µm, respectively. The indentation modulus was computed according to the Hertzian theory for spherical indentation [33,34] by fitting the force-penetration data achieved at equilibrium. Table 4 reports the details of the indentation tests.

Tissue permeability was identified by suitably adapting the analytical solution available for the vertical displacement of the top surface of a poroelastic layer subjected to load-controlled confined compression test proposed by Biot [35]. The analytical solution was used to fit the force-displacement data $h^j(\tau)$ collected during the spherical indentation, being *j* the load level. To this purpose, a dimensionless time τ^j has been introduced by following Oyen *et al.* [36] as

$$\tau^j = \frac{P^j_2 t}{\beta R h^j(t)}$$

Equation 1

where β is a parameter identified through numerical simulations and

P_2^j plays the role of a diffusivity. Then, a two-parameters (P_1^j and P_2^j) function is used to best fit the creep curves [37]:

$$h^j(\tau) = h^j(0) + P^j_1[g(\tau^j)]$$

Equation 2

where $h^j(0)$ is the indentation depth reached at the beginning of each holding phase and:

$$g(\tau) = 1 - \sum_{m=0}^{\infty} \frac{8}{(1+2)^4 \pi^4 \tau_R} \left[e^{-(1+2m)^2 \pi^2 (\tau - \tau_R)} - e^{-(1+2m)^2 \pi^2 \tau}\right]$$

Equation 3

Finally, permeability is obtained, for each load level j, as:

$$K^j = \frac{P^j_2}{M_{eq}}$$

Equation 4

Statistical analysis

Data are expressed as mean ± standard deviation (SD) and statistical analysis was performed using Student's *t*-test, unless indicated otherwise. For the histological scoring analysis of variance stratified for each item was used. Data were analyzed using GraphPad Prism v5.00 (GraphPad Software, CA, USA). In all cases, $p < 0.05$ was considered statistically significant.

Results

Both mpASCs & huASCs efficiently differentiate into osteogenic & chondrogenic lineages *in vitro*

mpASCs were isolated from seven minipigs with an average yield of $5.6 \times 10^4 \pm 1.4 \times 10^4$ cells/ml of raw adipose tissue, quite comparable to that obtained from

Table 3. **International cartilage repair society** II scoring system[†].

Histological parameters	Score
Tissue morphology (polarized light)	0: full-thickness collagen fibers; 100: normal cartilage birefringence
Matrix staining (metachromasia)	0: no staining; 100: full metachromasia
Cell morphology	0: no round/oval cells; 100: mostly round/oval cells
Chondrocyte clustering (four or more grouped cells)	0: present; 100: absent
Surface architecture	0: delamination or major irregularity; 100: smooth surface
Basal integration	0: no integration; 100: complete integration
Formation of tidemark	0: no calcification front; 100: tidemark
Subchondral bone abnormalities (marrow fibrosis)	0: abnormal; 100: normal marrow
Inflammation	0: present; 100: absent
Abnormal calcification/ossification	0: present; 100: absent
Vascularization (within the repaired tissue)	0: present; 100: absent
Surface/superficial assessment	0: total loss or complete destruction; 100: resembles intact articular cartilage
Mid/deep zone assessment	0: fibrous tissue; 100: normal hyaline cartilage
Overall assessment	0: bad (fibrous tissue); 100: good (hyaline cartilage)

[†]Reproduced from Mainil-Varlet *et al.* [32].

the human fat tissue used in this study (8.5×10^4 cells/ml) (Figure 2A). ASCs isolated from minipigs are smaller and with a more round shape when compared with human ASCs (Figure 2B), as we also previously described [25]. One week later, all the populations, started rapidly to grow with variable proliferation rates, as shown in Figure 2C. From passage 2 to 4, the average doubling time was 60.3 ± 16.5 h (range: 46.9–112.3 h) for the minipig cells, and it appears longer for the human ones (101.9 ± 22.8 h). mpASC clonogenic ability (16.1 ± 7.2%) was assessed between passage 2 and 4, and it was more pronounced than that determined for huASCs (10.1 ± 1.4%, see Figure 2A). To test their multidifferentiation potential *in vitro,* mpASCs and huASCs were induced by osteogenic and chondrogenic stimuli, and in suitable culture conditions for 2 and 3 weeks, respectively. *In vitro* osteo-differentiated ASCs significantly increased the osteogenic markers with respect to the control cells, such as ALP (Figure 3A), calcified extracellular matrix (Figure 3B) and collagen (Figure 3C) deposition of about 440, 151 and 110%, respectively for mpASCs, and of about 104, 152 and 401%, respectively for human cells. In addition, chondro-differentiated mpASCs and huASCs, grown

Table 4. Maximum load, load step size and total number of indentation sites for each sample type.

Sample	Tip radius R [μm]	Total load Fτ [mN]	Load steps	Indentation sites
Healthy control	25	0.9	0.1	8
Healthy control	400	1	0.1	6
OPF-A	25	0.7	0.1	3
OPF-A	400	1	0.1	4
OPF	25	1	0.1	4
OPF	400	1	0.1	4
UNT	25	0.3	0.1	5
UNT	400	0.6	0.1	4

OPF: Oligo(polyethylene glycol)fumarate; OPF-A: Oligo(polyethylene glycol)fumarate + autologous cells; UNT: Untreated.

Ⓐ

	mpASCs-1	mpASCs-2	mpASCs-3	mpASCs-4	mpASCs-5	mpASCs-6	mpASCs-7	huASCs
ASCs/ml raw adipose tissue	3.7×10^4	1.8×10^4	5.4×10^3	9.1×10^4	6.3×10^4	4.2×10^4	1.4×10^4	8.5×10^4
Mean clonogenicity % (P2-P4)	11.6 ± 3.1	17.5 ± 8.4	12.4 ± 2.3	30.5 ± 6.7	13.8 ± 2.4	9.96 ± 0.5	15.1 ± 0.2	10.1 ± 1.4

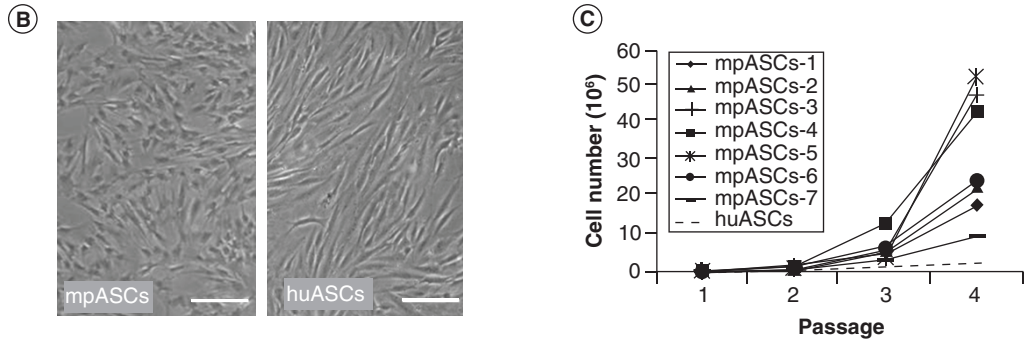

Figure 2. Isolation and characterization of minipig and human adipose-derived stem cells. (A) Cellular yield and clonogenic ability (expressed as percentage of number of colonies/number of plated cells) of mp- and hu-ASCs. **(B)** Cell morphology at passage 3 (optical microscopy, 40× magnification, scale bar 100 μm). **(C)** Proliferation of ASCs maintained in culture until passage 4 (plating 8×10^4 cells at passage 1).
ASC: Adipose-derived stem cell; huASC: Human adipose-derived stem cell; mpASC: Minipig adipose-derived stem cell.

in pellet culture for 21 days, increased the amount of GAGs compared with undifferentiated cells (92 and 28%, respectively) (Figure 3D).

Minipigs well tolerated the surgical procedures & the bio-constructs

After a short period of limping, lasting not more than 14 days from surgery, all the minipigs recovered a normal gait, without any functional limitations. Knee swelling was present in all the animals for about 3 weeks postsurgery.

OPF alone or in combination with ASCs improved MOCART scores

Magnetic resonance of all treated joints was performed immediately after the explant of the limbs, before the arthrotomy. As revealed by the modified 2D MOCART scale, MR confirmed the appropriateness of our severe critical defect model, as the untreated group reached only 25% of the repair rate, while the benefit of the use of both seeded and unseeded scaffolds was detectable. Indeed, all the scaffold-treated defects showed significantly higher scores in comparison to the untreated ones (Figure 4), with no differences among the OPF and OPF-ASC groups. Indeed, from a qualitative point of view, a mild scaffold resorption was observed in the scaffold groups: the defects were partially invaded by bone-like tissue, with some irregularities of the superficial layer. No bone absorption as well as no signs of edema were seen around the scaffold.

A good integration of the scaffold to the bone was observed, with no signs of reaction in the bone tissue around the implanted scaffold. Empty defects showed incomplete fibrous tissue filling, reaching no more than two-third of the original defect, covered by fibrotic tissue of low signal.

Following arthrotomy, joint inspection did not reveal any sign of inflammation, as well as adhesion, hypertrophy or fibrosis of synovial membrane. The surface of all defects showed small cylindrical lacks of substance, sometimes associated with signs of vascular infiltration (Figure 5, A2–5).

In only one animal signs of local infection were observed and it was excluded from the study to assure the reliability of the results. Out of the four defects of this minipig, two had been treated with allogeneic cells, one with OPF alone and one left empty. In this study, the arranged defects to be treated with allogeneic cells were three in total (Table 1); for this reason, even though no macroscopical and histological differences between the only retrieved OPF-Allo construct and the ones produced with autologous cells were observed, the data about this group are not shown and no statistical analysis was performed.

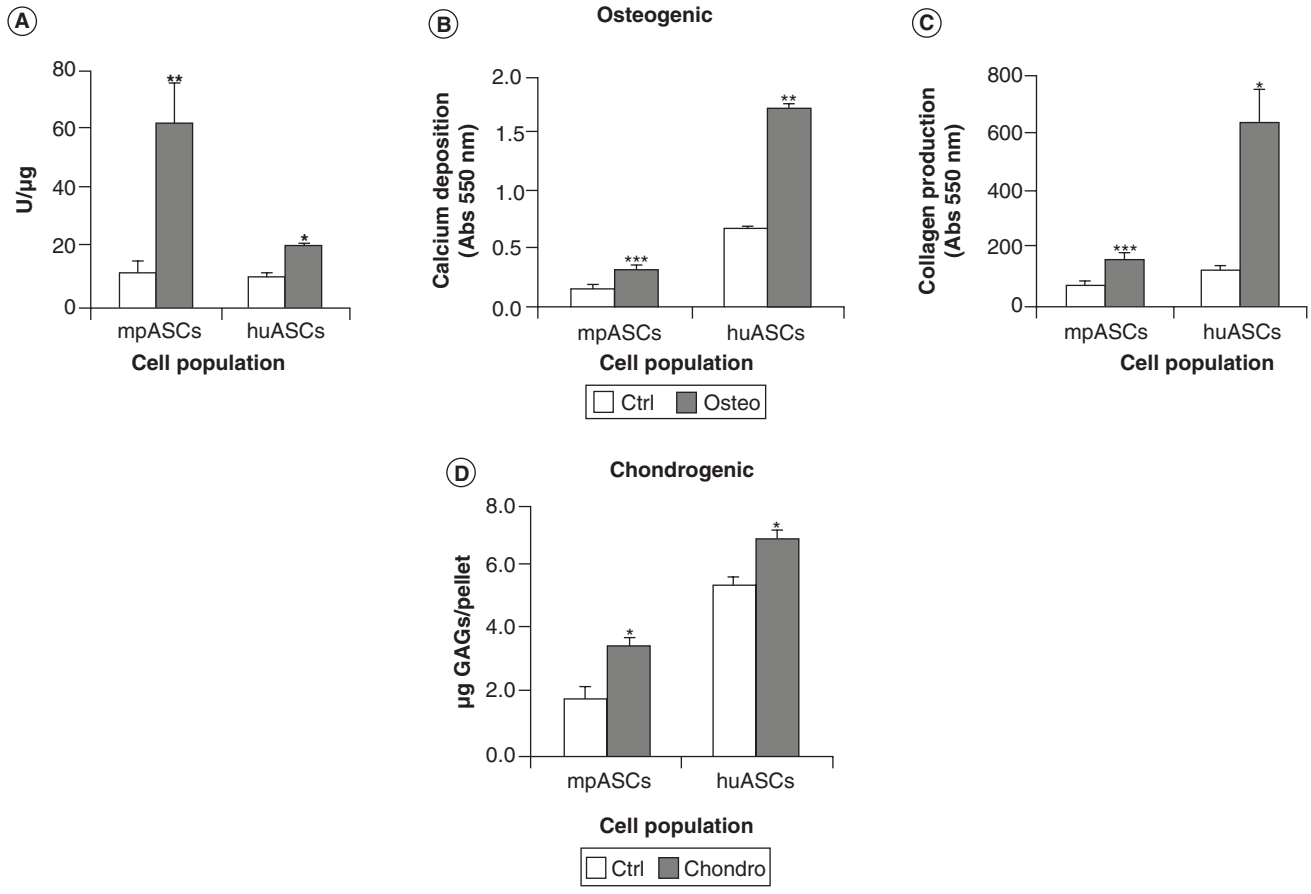

Figure 3. *In vitro* osteogenic and chondrogenic potential of adipose-derived stem cells. (A) Alkaline phosphatase activity (ALP), **(B)** calcified extracellular matrix and **(C)** collagen deposition of mp- and hu-ASCs cultured for 14 days in undifferentiated (white bars) and osteogenic (dark bars) medium (n = 7). Glycosaminoglycan quantification of undifferentiated (white bars) and chondro-differentiated (dark bars) **(D)** micromasses expressed as microgram of GAGs for each pellet, cultured for 21 days (n = 3). Data are expressed as mean ±SEM. Differentiated versus undifferentiated *p < 0.05, **p < 0.01, ***p < 0.001.
Chondro: Chondro-differentiated cell; Ctrl: Undifferentiated cell; huASC: Human adipose-derived stem cell: mpASC: Minipig adipose derived stem cell; Osteo: Osteo-differentiated cell.

ASCs seeded on OPF allowed the regeneration of more mature bone & the upregulation of collagen type II expression at cartilage level

In both unseeded and mp-ASC or hu-ASC seeded scaffolds most of the tissue present into the defects was fibrocartilage, mainly located in the central part of the defects (Figure 5, B3–5). In general, they were less intensely Safranin-O positive respect to the native articular cartilage (Figure 5, B1), showing a lower content of glycosaminoglycans (GAG). Cartilage was present only at the edge of the defects in all the scaffold-treated groups (Figure 5, B3–5). In terms of subchondral bone repair, a bone formation process was evident, with osteoblasts lining the surfaces of the construct, above all in OPF-A and OPF-Hu groups (Figure 5, C3–5). Interestingly, more mature bone, with the presence of bone lamellas, was observed in OPF-Hu-treated defects.

In the untreated defects, the repair tissue was characterized by a strong depletion of GAG content, as shown by the poorly intense Safranin-O staining; overall, it was constituted mainly by fibrous tissue, with blood vessels and a disorganized extracellular matrix, protruding into the defect cavity (cartilage-like tissue flow). Fibrocartilage was very scarcely represented (Figure 5, B2), and restoration of the subchondral bone was insufficient and very immature as it started with endochondral bone formation at the borders of the defect (Figure 5, C2).

Anyways, cartilage hypertrophy was not observed in any sample of the experimental groups.

As shown in the healthy joint (Figure 5, D1), analysis by polarized light microscopy allowed to evaluate the presence of the collagen components, of primary and secondary bone, the differentiation between mature and developing osteons and the bone lamellas and their

orientation. In the untreated group, collagen fibrils were not organized in lamellar form (Figure 5, D2), whereas in both seeded and unseeded OPF defects, an organized distribution of collagen fibrils was observed. In particular, the deposition of lamellar bone occurred within the pores of the scaffolds (Figure 5, D3–5), without any relevant differences among unseeded and mp-ASC or hu-ASC seeded scaffolds.

In the defects treated with both OPF-A and OPF-Hu a considerable quantity of collagen type II (COLL-II) was present (Figure 5, E4–5), and it was comparable to one of the healthy cartilage (Figure 5, E1). In contrast, the COLL-II immunostaining was much less evident in both untreated and unseeded OPF groups (Figure 5, E2–3). However, in all the groups, the inner part of the neocartilage of the repaired tissue contained scarce COLL-II immunostaining positive tissue (data not shown). In addition, the neo-formed bone was more positive for collagen type I in OPF-A and OPF-Hu groups in comparison to untreated and unseeded OPF groups (Figure 5, F2–5).

According to ICRS II scores, significant differences were found between OPF and OPF-A groups for some parameters. In particular, tidemark formation, vascularization, matrix staining, cell morphology and tissue morphology scored significantly higher in the group treated with OPF-A with respect to OPF ($p < 0.05$). Just surface assessment score was significantly lower in OPF-A compared with OPF. No other differences were found between the two scaffold groups. However, untreated group showed significantly higher scores for some parameters, including formation of tidemark, subchondral abnormalities and basal integration, as well as parameters concerning the surface assessment, suggesting that the presence of residual scaffold at the defect site negatively affected this kind of evaluations (Figure 6).

Neocartilage of OPF-A group showed biomechanical properties similar to the native tissue ones

The indentation modulus at equilibrium M_{eq}, standard deviation identified for healthy control, OPF-A, OPF and untreated samples are reported in Figure 7 for both the 25 μm (A) and 400 μm (B) tips.

R^2 fitting parameter was found in the following ranges. For the data (F_L-h_{eq}) measured using the 25 μm tip: [0.97–0.98], healthy cartilage and OPF-A samples; [0.92–0.93], OPF samples; [0.86–0.88], untreated samples. For the data (F_L-h_{eq}) measured using the 400 μm tip: [0.97–0.98], healthy cartilage and OPF-A samples; [0.89–0.91], OPF samples; [0.86–0.87], untreated samples.

In all cases, indentation moduli measured using the small tip radius is larger than those found with the large tip radius. Healthy cartilage exhibits an indentation modulus (603 ±199 kPa) similar than that found for OPF-A samples (545 ±96 kPa) with R_{25} tip. A similar consideration holds for the large tip radius: healthy cartilage and OPF-A samples exhibited an indentation modulus of 238 ±68 kPa and 272 ±29 kPa, respectively. Both OPF and untreated samples showed an indentation modulus at equilibrium significantly smaller than that found for healthy cartilage and OPF-A samples. In particular, M_{eq} for OPF sample was 268 ± 102 kPa and 110 ± 10 kPa for R_{25} and R_{400}, respectively (both $p < 0.05$ with respect to native cartilage and OPF-A group); M_{eq} for untreated sample was 292 ±47 kPa and 81 ±25 kPa for R_{25} and R_{400}, respectively (both $p < 0.05$ with respect to native cartilage and OPF-A group). No appreciable difference was found between OPF and untreated samples (Figure 7).

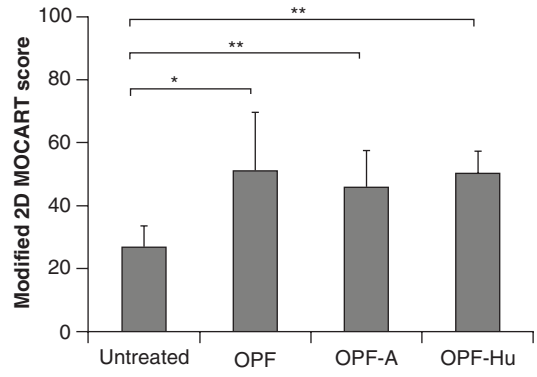

Figure 4. Modified 2D MOCART score obtained analyzing magnetic resonance imaging of the *ex vivo* osteochondral lesions.
*p < 0.05, **p < 0.01.
OPF: Unloaded scaffold; OPF-A: Oligo(polyethylene glycol)fumarate + autologous cells;
OPF-hu: Oligo(polyethylene glycol)fumarate seeded with human adipose-derived stem cells.

The tissue permeability k is identified for both indenter tips and for each load level. The k parameter was calculated for healthy and OPF-A samples only for which the creep response was fitted with R^2 values greater than 0.8. The OPF and untreated samples exhibited creep curves which were fitted with R^2 values lower than 0.7; therefore, the poroelastic fitting model was considered unsuited.

Averaged values of the tissue permeability over all the load levels are: $2.05 \pm 1.10 \times 10^{-15}$ for R_{400} and $9.08 \pm 0.68 \times 10^{-17}$ for R_{25} in case of healthy cartilage sample; $1.56 \pm 0.45 \times 10^{-15}$ for R_{400} and $1.38 \pm 1.11 \times 10^{-16}$ for R_{25} in case of OPF-A sample. In Figure 8, the decreasing trend of permeability is instead presented for both the samples (mean values are shown) with respect to the equivalent deformation, computed

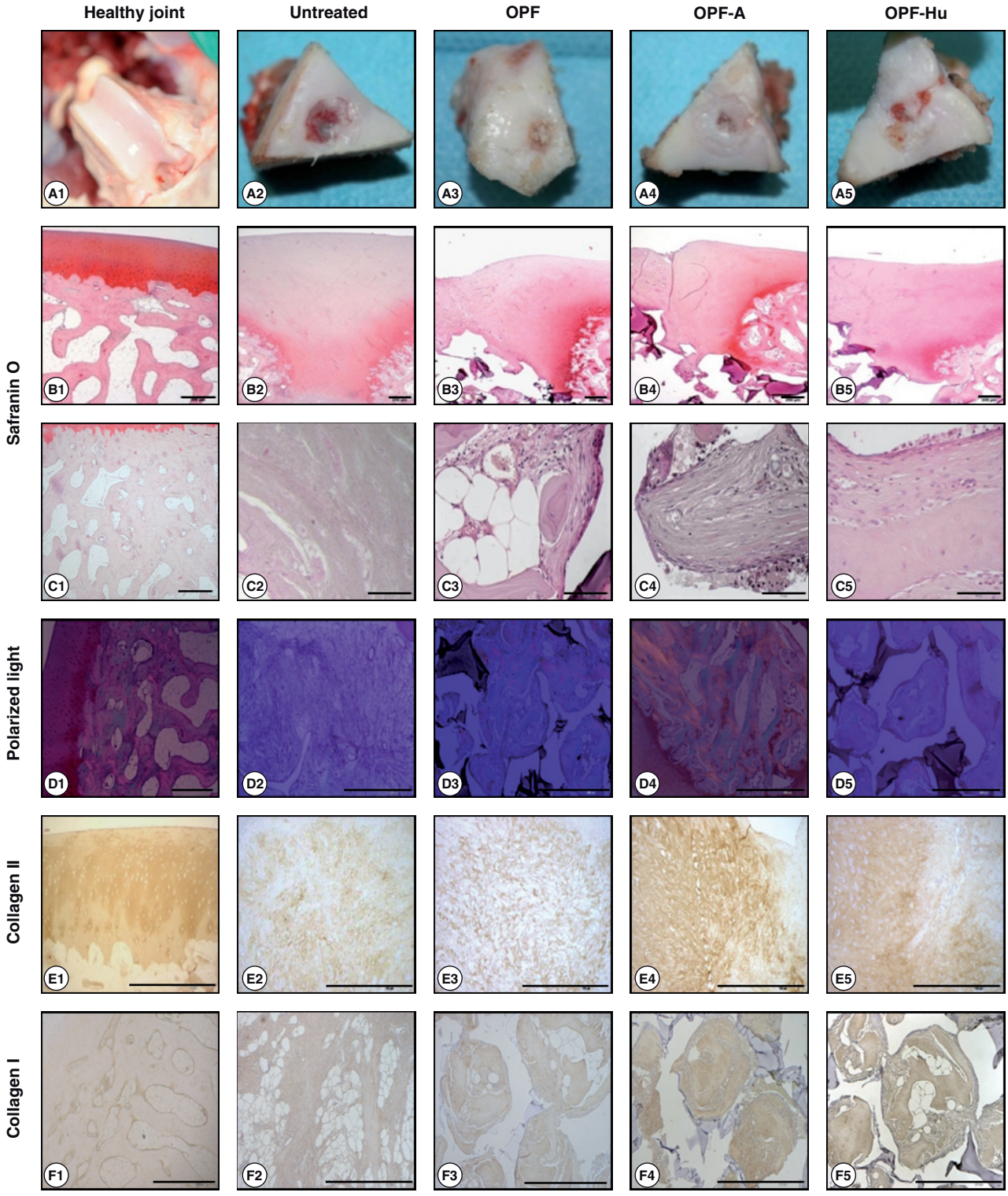

Figure 5. Gross appearance (row A) and histological sections (row B–F) of the neoformed osteochondral tissue of the different experimental groups after 6 months from implantation. Sections were stained with Safranin-O (row B: Cartilage layer, C: Bone layer), analyzed by polarized light microscope (row D) and immunostained with type II (row E) and type I (row F) anti-collagen antibodies. Scale bar: 50 μm for C2–C5, 200 μm for all the other pictures.
OPF: Oligo(polyethylene glycol) fumarate hydrogel; OPF-A: OPF + autologous cells; OPF-hu: OPF + human cells.

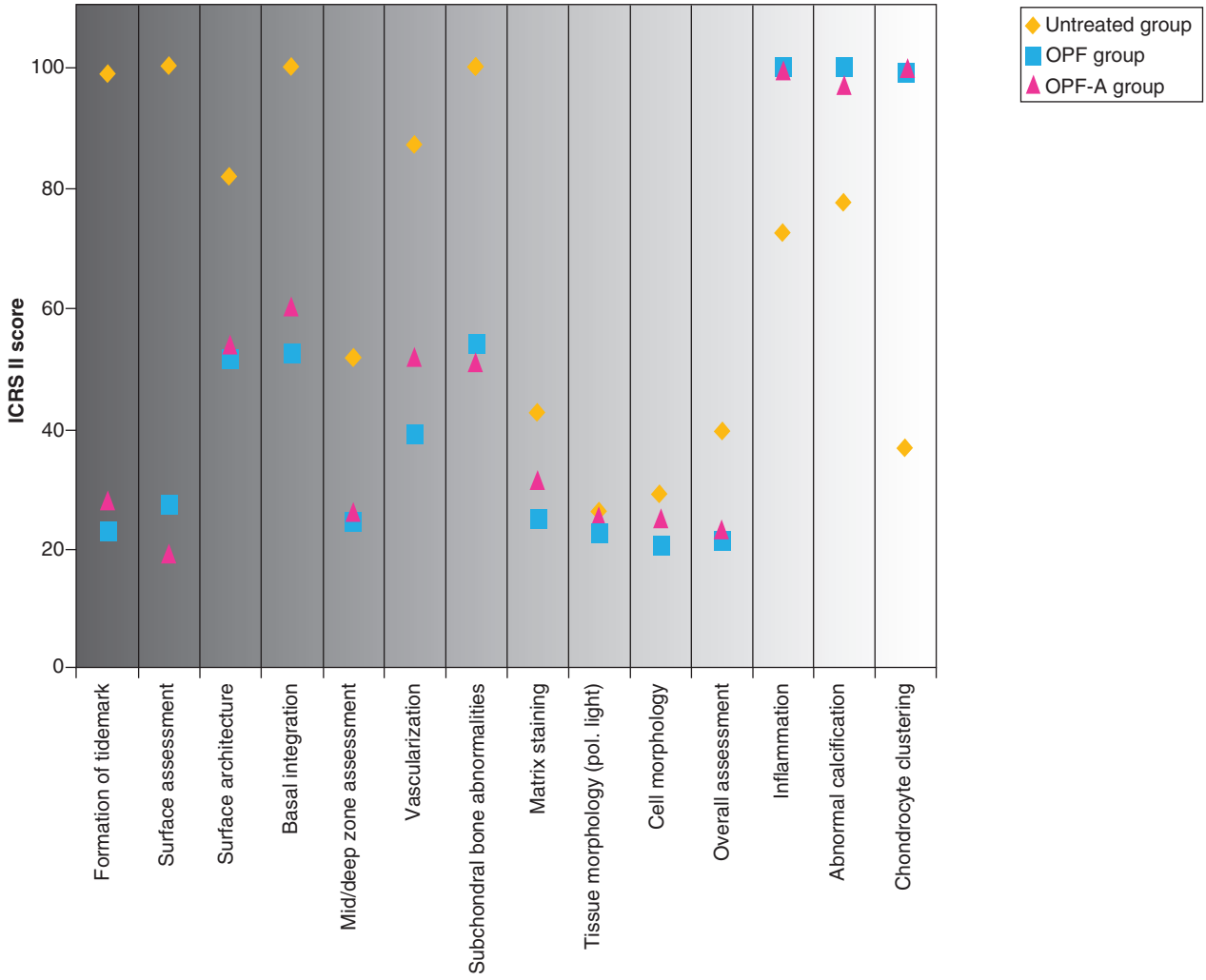

Figure 6. International Cartilage Repair Society II score of the neoformed osteochondral tissue of untreated, oligo(polyethylene glycol) fumarate hydrogel and oligo(polyethylene glycol) fumarate hydrogel and autologous cells groups. All the parameters included in the evaluation forms are depicted in the graph. Three different blind evaluators analyzed all the histological sections. OPF: Oligo(polyethylene glycol) fumarate hydrogel; OPF-A: Oligo(polyethylene glycol) fumarate hydrogel + autologous cells.

as the ratio between the current contact length and the indenter radius. Engineered construct appeared slightly less permeable at smaller deformation.

In Figure 9, normalized creep displacement h – ranging from 0 (instantaneous) to 1 (long term) – versus natural time and normalized time [36] are reported. Only selected curves are presented for the healthy cartilage (Figure 9A), OPF-A (Figure 9B) and OPF (Figure 9C) samples for both the two tips. A complete overlap between creep curves versus normalized time collected at different loads and different tip radii is found for the healthy cartilage and for the OPF-A samples. This indicates that fluid flow through the porous matrix is the main dissipation mechanism; whereas, the creep response of OPF could not be fitted with the poroelastic fitting function so, no creep curves versus normalized time are available (Figure 9C).

Discussion

In the last two decades, a wide variety of biological approaches have been proposed for the treatment of chondral and osteochondral defects, such as the use of multilayered scaffolds, enhanced or not by the use of progenitor cells or terminally differentiated chondrocytes, to provide a proper support to the different tissues [19–21,38]. Although these methods have shown promising results, they still have to be validated, and the development of an engineered graft before implantation to support an optimal repair needs further investigations. One of the main difficulties in selecting the most suitable approach is the great heterogeneity

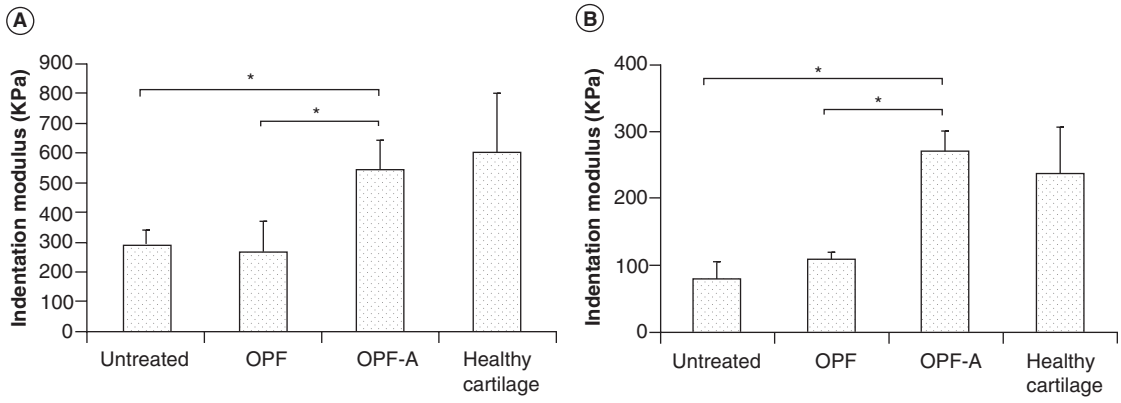

Figure 7. Biomechanical test of the neoformed osteochondral tissue by nanoindentation. Indentation modulus at equilibrium M_{eq} for untreated samples, OPF, OPF-A and healthy control and for the R_{25}**(A)** and R_{400} tip **(B)**. Data are expressed as mean ±SD.
OPF: Oligo(polyethylene glycol) fumarate hydrogel; OPF-A: Oligo(polyethylene glycol) fumarate hydrogel + autologous cells.

among the studies, including different animal models (mouse [39], rat [40], rabbit [41], sheep [18,42], pigs [21,39]), scaffolds and cell populations [20]. Moreover, size of the lesions and the followup duration are also parameters which differ considerably among studies [22,43].

OPF hydrogels have been previously well characterized and they have been shown to efficiently support bone regeneration [44]. A few reports concerning their use for osteochondral regeneration have been recently published. Hui *et al.* showed usefulness of OPF hydrogel for cartilage regeneration in a swine model [43]; in another study, bone marrow-derived mesenchymal stem cells, in association with OPF hydrogel, were used with satisfactory results to treat chondral defect (6 mm diameter, 1 mm depth) in a porcine model [22]. In our study, critical osteochondral defects were treated with a negatively charged SMA-modified OPF hydrogel combined with either autologous or human ASCs in immunocompetent minipigs. Adult animals were chosen to reduce the spontaneous reparative process occurring in younger subjects and thus to obtain results more comparable to human adults. Our findings show that, 6 months after implantation, expanded undifferentiated ASCs seeded on OPF hydrogel were able to improve the biomechanical properties of the newly formed cartilage with respect to the defects treated with OPF alone. Indeed only the neocartilage found in the cell-loaded scaffold groups displayed poroelastic behavior, as well as indentation modulus comparable to native cartilage. In particular, indentation modulus found for small tips was higher than that found with larger tips. This is consistent with previously published data and can be justified considering the microstructural architecture of the tissues which are loaded in different ways when applying different tip radii [45]. The permeability decrease with increasing strain is a well-known phenomenon, which can be easily justified by the change in porous architecture upon compression of the tissue. This creep response, in other words the overlapping of the normalized displacement versus normalized time, is consistent with a poroelastic dissipation mechanism involved in the fluid flow through the porous matrix. On the other hand, the creep response of OPF and untreated samples could not fit with the poroelastic interpolation function. This indicates that other dissipation mechanisms are involved in these samples in addition to the fluid-flow through the porous matrix.

Furthermore, although histological observations indicated that cartilage regeneration was still in progress in all the samples, the use of ASCs associated with scaffolds allowed an improvement in COLL-II expression, matrix staining, tissue and cell morphology and formation of

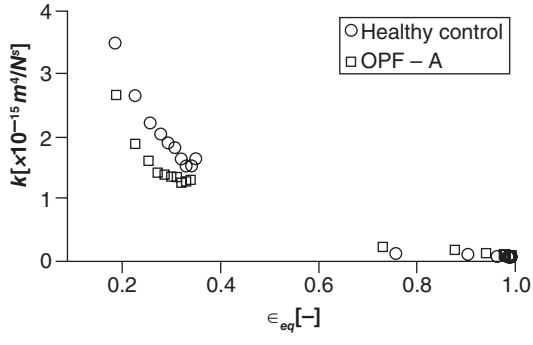

Figure 8. Mean permeability values with respect to the equivalent deformation of healthy control and OPF-A.
OPF-A: Oligo(polyethylene glycol) fumarate hydrogel + autologous cells.

tidemark compared with scaffolds alone. On the other hand, some parameters of ICRS II scale scored higher in the untreated lesions in comparison to the lesions treated with scaffolds, in particular those evaluating the surface quality. These data could be attributed to the lack of scaffold in this group that allowed the defects to be easily filled by amorphous tissue. Indeed, both radiological and histological analyses revealed that 6 months after implantation, scaffolds were still detected at the defect site. However, the untreated defects were fulfilled by fibrous unorganized tissue, characterized by very poor histological and biomechanical properties. Moreover, untreated defects showed a significantly lower signal intensity and worse scores in term of adhesion and effusion when compared with the defects treated with scaffold, as demonstrated by 2D-MOCART score based on magnetic resonance images.

Considering bone regeneration, defects, a more mature tissue characterized by a higher expression of collagen type I, compared with untreated or unseeded OPF groups, was observed in all the OPF+ASC defects. ASCs derived from several animal species, as well as from humans, have been shown to be able to differentiate into osteoblast-like cells *in vitro* [25,26,46] and to promote bone regeneration in animal models [13,14]. These properties may be related to the ASC multidifferentiation potential and to their pro-angiogenic ability [47] through the secretion of factors such as VEGF, HGF and TGF-β [48]. However, ASCs seemed to inhibit the vascularization process of newly formed cartilage, as evaluated by the ICRS II score. A possible explanation of this phenomenon could be that ASC can or cannot release angiogenic factors depending on the different cross-talk between them and the resident cells at the site of injury [49]. In our model, we used undifferentiated ASCs underwent to minimal manipulation in view of a possible easier way to translate this approach into the clinic. Moreover, this decision was also influenced by recent evidences on the mechanism of action of mesenchymal stem cells. Indeed, while at the beginning the attention was mainly focused on their ability to differentiate in specific cell lineages, more recently it was proposed that their therapeutic benefits are largely dependent on their ability to act as a drug store of trophic factors [50] and as modulators of immune response [51]. From this point of view, one of the main action of mesenchymal stem cells is to support resident cells, which most likely are the major effectors of the tissue regeneration. Moreover, several soluble mediators, able to promote angiogenesis, tissue regeneration and remodeling, immune cell activation or suppression and cellular recruitment, seem to be released according to the needs of the damaged environment [49]. For this reason we applied bioconstructs seeded with undifferentiated cells, which are known to react to the most proper

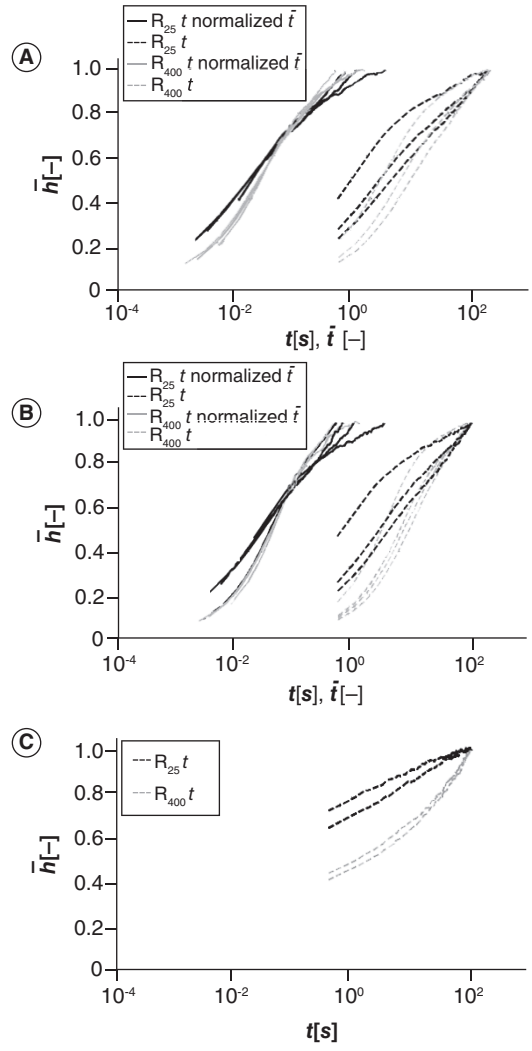

Figure 9. Creep curves for the healthy cartilage (A), OPF-A (B) and OPF (C) samples for both R_{25} (dark lines) and R_{400} (light lines) tips. In **(A)** and **(B)**, representative curves are shown with respect to natural time t (dotted lines) and dimensionless time t (continuous lines); in **(C)** only creep curves with respect to natural time are reported.

stimuli induced at the lesion site, without adding any other external stimuli, such as growth factors.

Undifferentiated MSCs express low levels of human leukocyte antigen (HLA) class I and II, that give them a so-called 'stealth' ability not to be recognized as not self by the host immune system in allogeneic implants [52]. Despite this feature it has been shown that in some cases MSCs were able to elicit an immune response in both animal studies and clinical trials [53,54]; on the other hand other studies support the feasibility and the effectiveness of the use of ASCs in allogeneic animal model [55,56].

In our study, no evident immune response has been detected; indeed all animals, monitored during the entire follow-up period, showed comparable clinical

outcome independently from the use of either human or autologous cells, confirming the low immunogenicity of ASCs.

From the effectiveness point of view, the slight differences between human and animal-derived ASCs [25] might represent a limit when translating preclinical data into clinical application. In this study, the effects elicited by autologous and human ASC-based bioconstructs were compared in order to provide informations about the behavior of both these cell types at the site of injury. Indeed, one of the most important criticism about their heterologous use is that cells could behave in a different way when they are in presence of xenostimuli (cytokines, growth factors, etc.), since the cross-talk between implanted and resident cells might be slightly distorted. However, although the limited number of defects treated with human ASCs, our data show that both autologous and human OPF+ASC constructs are able to ameliorate the subchondral bone and the newly formed biomechanical cartilage properties if compared with the scaffold alone. Interestingly, the more mature bone, characterized by the presence of very mature bone lamellas, was observed in defects treated with human bio-construct.

One of the limitations of our study concerns the cell seeding on OPF scaffolds; indeed, due to the limited number of defects, a cell dose-response study was not performed, as a fixed number of cells was seeded in all the defects. Although ASCs were not labeled, the differences in term of new tissue quality found between seeded and unseeded hydrogels support the hypothesis of a direct cell involvement in the regeneration process, probably mainly by means of their paracrine effect.

Conclusion

This study provides the evidence that both porcine and human adipose-derived stem cells associated to OPF hydrogel allow improving osteochondral defect regeneration. The swine model employed here confirmed to be reliable for testing regenerative strategies for osteochondral repair. Our data confirms the suitability of OPF as biomaterial for bone regeneration, whereas it seems to be not particularly prone to guide a proper chondral regeneration. This scarce effectiveness can be partially reverted by the combination of ASCs with the hydrogel, as demonstrated by the improvement of the mechanical properties of the newly formed cartilage. Various parameters, including scaffold pore dimensions, possible association with growth factors, number of cells and biodynamic construct formation, need to be considered before planning any clinical application of this model.

Future perspective

Due to their availability and low immunogenicity, ASCs represent an optimal mesenchymal cell type for regenerative purpose and their use has been already proposed for the treatment of different pathologies. However, the several concerns about their use still cause a gap between the preclinical studies and the clinical application. Studies in large animal model can

Executive summary

- The treatment of osteochondral defects still represents one of the most challenging issues in the orthopedic practice.
- The combined use of monophasic scaffolds and progenitor cells seems to be a promising approach.
- Adipose tissue is a smart source of mesenchymal stem cells characterized by good clonogenic ability, proliferation rate and multidifferentiation potential.

Methods

- Experimental osteochondral defects of minipigs' trochleas were treated with oligo (polyethylene glycol) fumarate (OPF) scaffold alone or preseeded with both autologous and human adipose-derived stem cells (ASCs). The outcome was evaluated after 6 months from surgery.

Results

- All the treatments based on the combination of both porcine and human ASCs and OPF hydrogel were safe and did not elicit any immune reaction.
- Both autologous and human ASCs seeded on OPF allow a better quality cartilage tissue regeneration with respect to unseeded scaffold, with improved biomechanical properties and higher collagen type II expression. In all cases, cartilage was not mature yet, probably because the regeneration process was slower than the expected since adult animals were used.
- Both autologous and human ASCs seeded on OPF allow the regeneration of more mature bone with upregulation of collagen type I expression.

Discussion

- Minipig represents an appropriate animal model to test tissue engineering-based treatments for severe osteochondral defects.
- This study supports the feasibility of the treatment of osteochondral defects with autologous or heterologous ASCs in association with OPF hydrogel, confirming the low immunogenicity of these cells.

help in filling this gap, as they can provide useful and reliable informations about the possible use of these cells in human. Our positive results allow to speculate the effectiveness of ASCs in combination with scaffolds also to repair severe osteochondral defects in patients with indications for this kind of treatment, although further confirmation needs to be achieved by specific clinical trials. Moreover, in the future to extend this treatment to the general population, it is also necessary to pass through an economical sustainability process.

Acknowledgements

The authors thank A Addis, M Campagnol, M Pamovio and M Melato for their very valid work with animal care and help in surgery; D Stanco and S Molinari for their help in the *in vitro* experiments; S Turolla, S Miliano and S Denti for their contribution in MRI evaluations; A Nonis for the statistical support.

Financial & competing interests disclosure

This work has been partially supported by the Italian Minis-try of Health. The authors have no other relevant affiliations or financial involvement with any organization or entity with a financial interest in or financial conflict with the subject matter or materials discussed in the manuscript apart from those disclosed.
No writing assistance was utilized in the production of this manuscript.

Ethical conduct of research

The authors state that they have obtained appropriate institu-tional review board approval or have followed the principles outlined in the Declaration of Helsinki for all human or animal experimental investigations. In addition, for investigations involving human subjects, informed consent has been obtained from the participants involved.

References

Papers of special note have been highlighted as:
• of interest; •• of considerable interest.

1 Madry H, van Dijk CN, Mueller-Gerbl M. The basic science of the subchondral bone. *Knee Surg. Sports Traumatol. Arthrosc.* 18, 419–433 (2010).

•• **Provides insights into the anatomy, morphology and pathology of the subchondral bone; its deep knowledge is fundamental in the cartilage repair setting, as articular cartilage defects often arise from or extend into the subchondral bone.**

2 Hoshino A, Wallace WA. Impact-absorbing properties of the human knee. *J. Bone Joint Surg. Br.* 69, 807–811 (1987).

3 Mahjoub M, Berenbaum F, Houard X. Why subchondral bone in osteoarthritis? The importance of the cartilage bone interface in osteoarthritis. *Osteoporos. Int.* 23(Suppl. 8), S841–S846 (2012).

4 Madry H, Grun UW, Knutsen G. Cartilage repair and joint preservation: medical and surgical treatment options. *Dtsch Arztebl. Int.* 108, 669–677 (2011).

5 Pape D, Filardo G, Kon E, van Dijk CN, Madry H. Disease-specific clinical problems associated with the subchondral bone. *Knee Surg. Sports Traumatol. Arthrosc.* 18, 448–462 (2010).

6 Foldager CB. Advances in autologous chondrocyte implantation and related techniques for cartilage repair. *Dan. Med. J.* 60, B4600 (2013).

7 Lee KT, Kim JS, Young KW *et al.* The use of fibrin matrix-mixed gel-type autologous chondrocyte implantation in the treatment for osteochondral lesions of the talus. *Knee Surg. Sports Traumatol. Arthrosc.* 21, 1251–1260 (2013).

8 Pittenger MF, Mackay AM, Beck SC *et al.* Multilineage potential of adult human mesenchymal stem cells. *Science* 284, 143–147 (1999).

9 Zuk PA, Zhu M, Ashjian P *et al.* Human adipose tissue is a source of multipotent stem cells. *Mol. Biol. Cell* 13, 4279–4295 (2002).

10 Fukuchi Y, Nakajima H, Sugiyama D, Hirose I, Kitamura T, Tsuji K. Human placenta-derived cells have mesenchymal stem/progenitor cell potential. *Stem Cells* 22, 649–658 (2004).

11 Lu LL, Liu YJ, Yang SG *et al.* Isolation and characterization of human umbilical cord mesenchymal stem cells with hematopoiesis-supportive function and other potentials. *Haematologica* 91, 1017–1026 (2006).

12 Qi Y, Zhao T, Xu K, Dai T, Yan W. The restoration of full-thickness cartilage defects with mesenchymal stem cells (MSCs) loaded and cross-linked bilayer collagen scaffolds on rabbit model. *Mol. Biol. Rep.* 39, 1231–1237 (2012).

13 de Girolamo L, Arrigoni E, Stanco D *et al.* Role of autologous rabbit adipose-derived stem cells in the early phases of the repairing process of critical bone defects. *J. Orthop. Res.* 29, 100–108 (2011).

• **Highlights the usefulness of a cell-scaffold construct involving adipose-derived stem cells not predifferentiated *in vitro* for critical-size bone defect repair in an animal model.**

14 Park BH, Zhou L, Jang KY *et al.* Enhancement of tibial regeneration in a rat model by adipose-derived stromal cells in a PLGA scaffold. *Bone* 51, 313–323 (2012).

15 Melief SM, Zwaginga JJ, Fibbe WE, Roelofs H. Adipose tissue-derived multipotent stromal cells have a higher immunomodulatory capacity than their bone marrow-derived counterparts. *Stem Cells Transl. Med.* 2, 455–463 (2013).

16 Liu GB, Cheng YX, Feng YK *et al.* Adipose-derived stem cells promote peripheral nerve repair. *Arch. Med. Sci.* 7, 592–596 (2011).

17 Gutierrez-Fernandez M, Rodriguez-Frutos B, Ramos-Cejudo J *et al.* Effects of intravenous administration of allogenic bone marrow- and adipose tissue-derived mesenchymal stem cells on functional recovery and brain repair markers in experimental ischemic stroke. *Stem Cell Res. Ther.* 4, 11 (2013).

18 Kon E, Delcogliano M, Filardo G *et al.* Orderly osteochondral regeneration in a sheep model using a novel

nano-composite multilayered biomaterial. *J. Orthop. Res.* 28, 116–124 (2010).

19 Kim K, Lam J, Lu S *et al.* Osteochondral tissue regeneration using a bilayered composite hydrogel with modulating dual growth factor release kinetics in a rabbit model. *J. Control. Release* 168, 166–178 (2013).

20 Martin I, Miot S, Barbero A, Jakob M, Wendt D. Osteochondral tissue engineering. *J. Biomech.* 40, 750–765 (2007).

21 Schek RM, Taboas JM, Segvich SJ, Hollister SJ, Krebsbach PH. Engineered osteochondral grafts using biphasic composite solid free-form fabricated scaffolds. *Tissue Eng.* 10, 1376–1385 (2004).

22 Lim CT, Ren X, Afizah MH *et al.* Repair of osteochondral defects with rehydrated freeze-dried oligo[poly(ethylene glycol) fumarate] hydrogels seeded with bone marrow mesenchymal stem cells in a porcine model. *Tissue Eng. Part A.* 19, 1852–1861 (2013).

23 Nathan S, Das De S, Thambyah A, Fen C, Goh J, Lee EH. Cell-based therapy in the repair of osteochondral defects: a novel use for adipose tissue. *Tissue Eng.* 9, 733–744 (2003).

24 Jo S, Shin H, Mikos AG. Modification of oligo(poly(ethylene glycol) fumarate) macromer with a GRGD peptide for the preparation of functionalized polymer networks. *Biomacromolecules* 2, 255–261 (2001).

25 Arrigoni E, Lopa S, de Girolamo L, Stanco D, Brini AT. Isolation, characterization and osteogenic differentiation of adipose-derived stem cells: from small to large animal models. *Cell Tissue Res.* 338, 401–411 (2009).

26 de Girolamo L, Lopa S, Arrigoni E, Sartori MF, Baruffaldi Preis FW, Brini AT. Human adipose-derived stem cells isolated from young and elderly women: their differentiation potential and scaffold interaction during in vitro osteoblastic differentiation. *Cytotherapy* 11, 793–803 (2009).

27 de Girolamo L, Sartori MF, Arrigoni E *et al.* Human adipose-derived stem cells as future tools in tissue regeneration: osteogenic differentiation and cell-scaffold interaction. *Int. J. Artif. Organs* 31, 467–479 (2008).

28 Brini AT, Niada S, Lambertini E *et al.* Chondrogenic potential of human mesenchymal stem cells and expression of slug transcription factor. *J. Tissue Eng. Regen. Med.* doi:10.1002/term.1772 (2013) (Epub ahead of print).

29 Goebel L, Orth P, Muller A *et al.* Experimental scoring systems for macroscopic articular cartilage repair correlate with the MOCART score assessed by a high-field MRI at 9.4 T--comparative evaluation of five macroscopic scoring systems in a large animal cartilage defect model. *Osteoarthritis Cartilage* 20, 1046–1055 (2012).

30 Marlovits S, Singer P, Zeller P, Mandl I, Haller J, Trattnig S. Magnetic resonance observation of cartilage repair tissue (MOCART) for the evaluation of autologous chondrocyte transplantation: determination of interobserver variability and correlation to clinical outcome after 2 years. *Eur. J. Radiol.* 57, 16–23 (2006).

31 Hoemann CD, Chen G, Marchand C *et al.* Scaffold-guided subchondral bone repair: implication of neutrophils and alternatively activated arginase-1+ macrophages. *Am. J. Sports Med.* 38, 1845–1856 (2010).

32 Mainil-Varlet P, Van Damme B, Nesic D, Knutsen G, Kandel R, Roberts S. A new histology scoring system for the assessment of the quality of human cartilage repair: ICRS II. *Am. J. Sports Med.* 38, 880–890 (2010).

•• **First describes a validated scoring system for the evaluation of the quality of repaired cartilage from biopsy specimens based on histological observation.**

33 Johnson KL. *Contact Mechanics.* Cambridge University Press. Cambridge, UK (1985).

34 Field JS, Swain MV. A simple predictive model for spherical indentation. *J. Mater. Res.* 8, 297–306 (1993).

35 Biot MA. Theory of elasticity and consolidation for a porous anisotropic solid. *J. Appl. Phys.* 26, 182–185 (1955).

•• **This is a fundamental work which lays the basis for the analysis of the time-dependent behavior of poroelastic anisotropic solids and it evaluates analytically the case of compression test.**

36 Oyen M, Shean T, Strange D, Galli M. Size effect in indentation of hydrated biological tissues. *J. Mater. Res.* 27, 245–255 (2012).

• **This is one of the first works in which the dependence of the mechanical properties of hydrated biological tissues on the characteristic lengths of the experiment is quantitatively assessed with specific reference to indentation tests.**

37 Taffetani M, Gastaldi D, Gottardi R, Raiteri R, Vena P. Poroelastic response of articular cartilage by nanoindentation creep tests at different characteristic lengths. *Med. Eng. Phys.* 36, 850–858 (2014).

38 Duan P, Pan Z, Cao L *et al.* The effects of pore size in bilayered poly(lactide-co-glycolide) scaffolds on restoring osteochondral defects in rabbits. *J. Biomed. Mater. Res. A.* doi: 10.1002/jbm.a.34683 (2013) (Epub ahead of print).

39 Peretti GM, Xu JW, Bonassar LJ, Kirchhoff CH, Yaremchuk MJ, Randolph MA. Review of injectable cartilage engineering using fibrin gel in mice and swine models. *Tissue Eng.* 12, 1151–1168 (2006).

40 Gao J, Dennis JE, Solchaga LA, Awadallah AS, Goldberg VM, Caplan AI. Tissue-engineered fabrication of an osteochondral composite graft using rat bone marrow-derived mesenchymal stem cells. *Tissue Eng.* 7, 363–371 (2001).

41 Schaefer D, Martin I, Jundt G *et al.* Tissue-engineered composites for the repair of large osteochondral defects. *Arthritis Rheum.* 46, 2524–2534 (2002).

42 Kandel RA, Grynpas M, Pilliar R *et al.* Repair of osteochondral defects with biphasic cartilage-calcium polyphosphate constructs in a sheep model. *Biomaterials* 27, 4120–4131 (2006).

43 Hui JH, Ren X, Afizah MH, Chian KS, Mikos AG. Oligo[poly(ethylene glycol)fumarate] hydrogel enhances osteochondral repair in porcine femoral condyle defects. *Clin. Orthop. Relat. Res.* 471, 1174–1185 (2013).

• **Describes the improvement of cartilage regeneration in a micropig model of cartilage defect using**

Oligo[poly(ethylene glycol)fumarate] hydrogel but also suggests the requirement of combining this scaffold with other 'tissue-regenerating mediators' to ameliorate its regenerative capability.

44 Dadsetan M, Giuliani M, Wanivenhaus F, Brett Runge M, Charlesworth JE, Yaszemski MJ. Incorporation of phosphate group modulates bone cell attachment and differentiation on oligo(polyethylene glycol) fumarate hydrogel. *Acta Biomater.* 8, 1430–1439 (2012).

45 Simha NK, Jin H, Hall ML, Chiravarambath S, Lewis JL. Effect of indenter size on elastic modulus of cartilage measured by indentation. *J. Biomech. Eng.* 129, 767–775 (2007).

46 Niada S, Ferreira LMJ, Arrigoni E *et al.* Porcine adipose-derived stem cells from buccal fat pad and subcutaneous adipose tissue for future preclinical studies in oral surgery. *Stem Cell Res. Ther.* 4, 148 (2013).

47 Rubina K, Kalinina N, Efimenko A *et al.* Adipose stromal cells stimulate angiogenesis via promoting progenitor cell differentiation, secretion of angiogenic factors, and enhancing vessel maturation. *Tissue Eng. Part A.* 15, 2039–2050 (2009).

48 Rehman J, Traktuev D, Li J *et al.* Secretion of angiogenic and antiapoptotic factors by human adipose stromal cells. *Circulation.* 109, 1292–1298 (2004).

49 Dimarino AM, Caplan AI, Bonfield TL. Mesenchymal stem cells in tissue repair. *Front. Immunol.* 4, 201 (2013).

50 Caplan AI, Dennis JE. Mesenchymal stem cells as trophic mediators. *J. Cell. Biochem.* 98, 1076–1084 (2006).

51 Gonzalez MA, Gonzalez-Rey E, Rico L, Buscher D, Delgado M. Treatment of experimental arthritis by inducing immune tolerance with human adipose-derived mesenchymal stem cells. *Arthritis Rheum.* 60, 1006–1019 (2009).

52 Yanez R, Lamana ML, Garcia-Castro J, Colmenero I, Ramirez M, Bueren JA. Adipose tissue-derived mesenchymal stem cells have *in vivo* immunosuppressive properties applicable for the control of the graft-versus-host disease. *Stem Cells* 24, 2582–2591 (2006).

53 Hare JM, Fishman JE, Gerstenblith G *et al.* Comparison of allogeneic vs autologous bone marrow-derived mesenchymal stem cells delivered by transendocardial injection in patients with ischemic cardiomyopathy: the POSEIDON randomized trial. *JAMA* 308, 2369–2379 (2012).

54 Huang XP, Sun Z, Miyagi Y *et al.* Differentiation of allogeneic mesenchymal stem cells induces immunogenicity and limits their long-term benefits for myocardial repair. *Circulation* 122, 2419–2429 (2010).

55 Sacerdote P, Niada S, Franchi S *et al.* Systemic administration of human adipose-derived stem cells reverts nociceptive hypersensitivity in an experimental model of neuropathy. *Stem Cells Dev.* 22, 1252–1263 (2013).

56 Zhu W, Shi XL, Xiao JQ, Gu GX, Ding YT, Ma ZL. Effects of xenogeneic adipose-derived stem cell transplantation on acute-on-chronic liver failure. *Hepatobiliary Pancreat. Dis. Int.* 12, 60–67 (2013).